Experimental Mechanics (2008) 48:789–798
DOI 10.1007/s11340-008-9136-2

Thermoplastic Polymer Shrinkage in Emerging Molding Processes

A.L. Gershon · L.S. Gyger Jr. · H.A. Bruck · S.K. Gupta

Received: 6 October 2007 / Accepted: 3 March 2008 / Published online: 8 April 2008

Abstract In this paper, in situ experiments have been designed using the full-field deformation technique of Digital Image Correlation (DIC) to characterize non-uniform shrinkage in thermoplastic polymers commonly used in traditional and emerging molding processes. These experiments are capable of characterizing the differences in strains that develop due to thermal gradients and stiction as the polymer shrinks from the molten to the solid state during molding processes. The experimental set-up consists of simulated open molds, a heating stage, thermocouples for temperature measurements, and a video imaging system for DIC. From these experiments, it has been shown that there is a large increase in shrinkage strain associated with the transition of the polymer from the molten to the solid state in a mold with reduced side rigidity, and as it is cooled below the Vicat softening point. Changing the cooling rate from air-cooled to quasi-steady state can eliminate the transition at the Vicat softening point. Furthermore, substantial decreases in shrinkage strain are observed when the polymer is melted in an open mold without mold release, while using mold release produces results similar to that observed with reduced side rigidity. A simple 1D model reasonably explains and predicts the observed trends in the shrinkage behavior due to temperature differences through the thickness of the polymer melt when using high conductivity molds as well as constraint in the polymer melt near the mold resulting from stiction.

Keywords Thermomechanical characterization · Multi-stage molding processes · Digital image correlation · Thermoplastic polymers · Shrinkage

A.L. Gershon (SEM Member) · L.S. Gyger Jr. · H.A. Bruck (✉, SEM Member) · S.K. Gupta
Department of Mechanical Engineering, University of Maryland, College Park, MD 20742, USA
e-mail: bruck@eng.umd.edu

Introduction

Characterization of shrinkage is an important aspect of effectively utilizing different molding processes. Traditional molding processes use rigid molds made out of aluminum or steel. These molds are also thermally highly conducting. Recently a new class of molding processes has emerged. These processes are called multi-material molding or multi-stage molding [1–4]. In these molding processes, prefabricated (or premolded) components are loaded into a mold and the material is molded on the top of these pieces. Hence, these components subsequently act as mold pieces during the molding process. Often these components are made out of polymers, and hence are significantly softer compared to steel or aluminum mold pieces. In addition, these components often have lower thermal conductivities and stiction. Recent experimental studies have shown that the shrinkage values are fundamentally different as a result of the presence of these soft and insulating mold pieces [5]. Therefore, we need to develop a fundamental understanding of the influence of thermal conductivity, rigidity, and stiction on the transient interaction of the mold and polymer melt. Developing such a fundamental understanding will be crucial to utilizing these emerging molding processes.

The shrinkage response of molded polymer components during the molding process has been found to impact the performance of the component. Residual stress can develop during the molding process, which introduces defects and/or reduces the longevity of molded components [6]. Therefore, it is important to characterize the shrinkage response of the polymer melt as it solidifies during the molding process in order to develop appropriate models for predicting shrinkage and the residual stresses associated with a particular component design and set of processing conditions [7].

Existing computational and experimental research efforts have focused on developing models capable of predicting shrinkage as a function of processing conditions. These efforts have explored how processing parameters such as injection pressure, packing pressure, holding pressure, melt temperature, and mold temperature affect shrinkage [6, 8–12]. Different thermoplastic materials will also exhibit different shrinkage characteristics. For example, models have been developed that describe how different material properties, such as crystallinity and viscosity, can affect shrinkage [13]. Shrinkage has been found to be highly anisotropic and shrinkage in the thickness direction is found to be significantly different than the flow direction [7, 14, 15]. Recent investigations have explored how the mold deformation affects the shrinkage [15]. It has been observed that higher injection pressures can significantly lower the observed values of shrinkage. Products with different geometries exhibit different shrinkage characteristics due to different constraints imposed by the mold pieces on the shrinking parts. Investigations have been conducted to explore how certain classes of highly specialized geometric shapes shrink during the injection molding cycle [11]. Experiments have also been conducted to determine how molded multi-material interface shapes influence the fracture resistance of the interface [16].

Efforts to characterize shrinkage in traditional molding processes assume rigid and highly conductive mold pieces. Currently, a better understanding is needed of the shrinkage behavior of thermoplastic polymers in molding in order to utilize emerging molding concepts, such as multi-stage multi-material molding, embedding of electronic components, and use of advanced polymer composites [1–3, 17–19]. For example, shrinkage of a polymer around an embedded electronic component during processing induces residual stresses that accelerate fatigue [17]. Also, in a multi-stage molding process, polymers are molded on top of each other altering the interaction between the mold and polymer melts [5]. There are ways to control the shrinkage response of the polymer by changing materials, component geometry, or processing conditions [8, 9]. However, models must be developed that relate these processing parameters to the thermal and thermomechanical residual stress distributions [7, 14, 20].

In order to characterize the shrinkage of thermoplastic polymers during molding processes, in-situ experiments have been developed for the first time using an open-mold design. The full-field deformation technique of Digital Image Correlation (DIC) is used to determine the displacement and strain fields on the surface of a polymer melt while cooling in the mold. The shrinkage response of a model thermoplastic polymer, low density polyethylene, is studied by simulating three different molding conditions representing high and low levels of stiction between the mold and polymer melt, high and low levels of mold support for the polymer melt, and high and low cooling rates associated with high and low thermal conductivity for the molds.

Experimental Procedure

Open Mold Configuration for Characterizing Shrinkage Response of Polymers

To characterize the shrinkage response of thermoplastic polymers during molding processes, an open mold configuration has been designed that permits variation of molding boundary conditions and thermal processing conditions. It has been designed to provide direct characterization of the difference in strains that arise due to thermal gradients and stiction of the polymer melt while cooling during a molding process, and can produce results that would be considered valid in the case of very low thermal conductivity molds with very low molding pressures. This configuration (seen in Fig. 1) consists of four components: (1) a heating stage (Thermolyne Nuova II Stir Plate), (2) an open mold into which either polymer pellets or hot-pressed polymers can be inserted (Pyrex Petri dish or aluminum plate), (3) a thermocouple (Omega HH560R digital thermometer) to obtain the temperature of the specimen during processing, and (4) a video imaging system that is used to acquire speckle patterns on the surface of the specimen during processing (1.3 megapixel Qimaging Retiga 1300 monochrome camera with a Nikon Micro-Nikkor 105 ml lens). The experimental setup is similar to a previously developed configuration for thermomechanical characterization during a welding process [21].

Full-field Displacement and Strain Analysis using Digital Image Correlation

To analyze the data from the video imaging system, the full-field deformation measurement technique of two-dimensional (2D) Digital Image Correlation (DIC) was used to calculate the displacement and corresponding strain fields from the surface of the polymer melt. Before each experiment, black spray paint was carefully applied to the top of the LDPE melt to obtain a random speckle pattern for DIC. The pattern has a mean speckle size of 15 pixels^2 and a density of 1 speckle/50 pixels^2, which was found to not change with time as determined by DIC measurements and provided reasonable levels of accuracy for the DIC technique [26]. Proper lighting was obtained with a fiber optic light source, and adjusted to obtain a Gaussian histogram across 256 gray levels during the experiments.

During each experiment, the polymer was first heated up to a maximum temperature of 225°C as determined by a thermocouple placed on or near the edge of the polymer

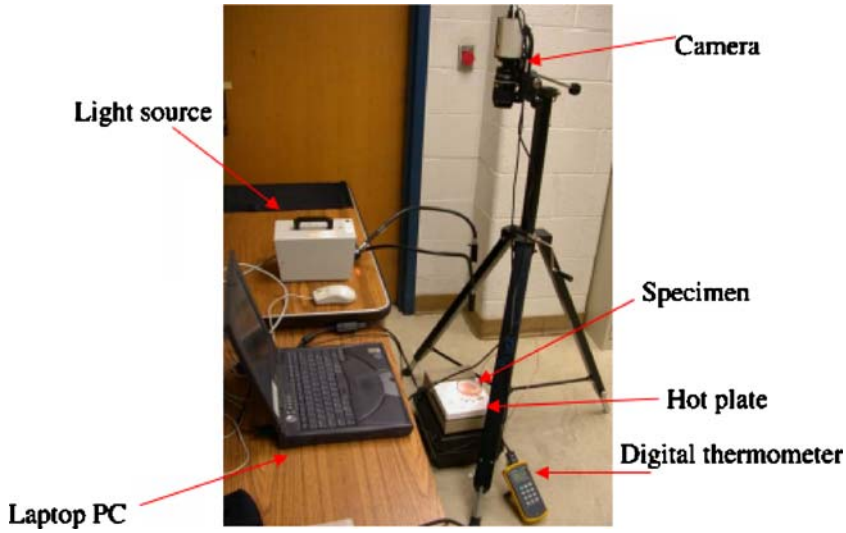

Fig. 1 New open-mold experimental configuration designed to characterize the in situ shrinkage response of thermoplastic polymers during molding processes

melt, and then thermally stabilized for at least 5 min before acquiring 8-bit gray scale images at a high frequency (30 s per image) upon cooling using VicSnap software from Correlated Solutions, Inc. (Columbia, SC). The acquisition frequency was gradually reduced to 8 min per image as the cooling rate decreased, as indicated on the typical experimental thermal profile in Fig. 2. Image acquisition is synced with thermocouple measurements obtained via an RS-232 input. In most cases the change in temperature between images was somewhere between 2°C and 4°C until approximately 70°C was reached where the change in temperature was between 5°C and 8°C. The 2D DIC technique determines orthogonal in-plane displacements (referred to as u and v) between images by tracking the random speckles to a high degree of accuracy though computer automated pattern recognition. The pattern recognition is accomplished by correlating a subset of pixels of one image (referred to as "undeformed") with their corresponding locations on a second image (referred to as "deformed") that is reconstructed via cubic B-spline interpolation in order to obtain a sub-pixel displacement associated with the center of the subset [22].

To analyze images obtained from each of the cases, the DIC software known as VIC-2D version 4.4.2 from Correlated Solutions was used. The in-plane displacements obtained from the subsets were fitted with polynomials or spline fits to obtain the normal strain fields, in the x direction (shown as ε_{xx}), which is referred to as the horizontal strain, in the y direction (shown as ε_{yy}), which is referred to as the vertical strain, and the shear strain (shown as ε_{xy}) [23]. An area-of-interest (AOI) with a diameter of 100 pixels was chosen in the center of the specimen, and 101 pixel square subset sizes were used with a step size of 5 pixels between subsets to correlate the displacements. Strains were obtained using polynomial fits to displacements obtained from a neighborhood of 15 data points around a given subset location.

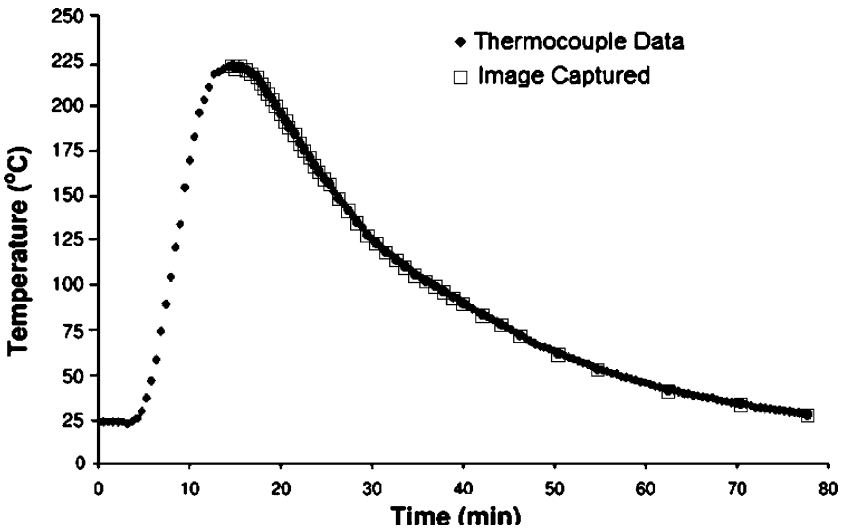

Fig. 2 Typical thermal profile associated with an in situ molding experiment using LDPE and air cooling in a Pyrex Petri dish, along with the times as which images were captured

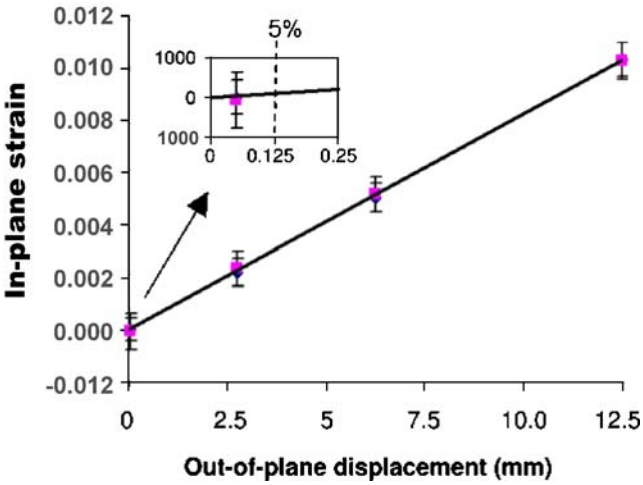

Fig. 3 Effect of out-of-plane displacement on 2D in-plane strain, and response in region associated with a 5% strain for a 2.5 mm thick specimen

Since the DIC technique that was employed is 2D, no information about the out-of-plane displacement associated with shrinkage is obtained. However, experiments were conducted to determine the effect of out-of-plane displacements on the 2D in-plane displacement fields due to the optical configuration of the video imaging system. Using a translation stage to displace a specimen out-of-plane, it was possible to characterize the artificial in-plane strains that develop due to defocusing of the images when the depth of field is exceeded (Fig. 3). Results obtained at a magnification of approximately 15.3 pixels/mm indicated that the in-plane strain error for 0.125 mm of out-of-plane displacement would be less than 500 μstrain, which was within the error range for the strains measured in this experiment. The corresponding level of out-of-plane shrinkage is 5% strain for a 2.5 mm thick specimen, which far exceeds the shrinkage expected for standard thermoplastic polymers. Thus, it was determined that the 2D DIC technique would be adequate for shrinkage characterization in the molding experiments. However, if the effect of the out-of-plane displacement on the apparent 2D in-plane displacements were to exceed this level, the three-dimensional (3D) DIC technique could be alternatively employed [24, 25].

Specimen Preparation

In order to characterize the effects that static frictional (i.e., stiction) aspects of molds will have on the shrinkage of a thermoplastic polymer during the molding process, three cases representing different levels of stiction, mold thermal conductivity, and mold side rigidity were studied: (a) high thermal conductivity molds with low stiction and substantially reduced side rigidity which simulate less rigid open mold side boundary associated with a compliant, low thermal conductivity previously molded component in a multi-stage molding process while one side remains a high thermal conductivity molding material (*case 1*), (b) low thermal conductivity molds with high side rigidity associated with traditional molding conditions and high stiction because of the absence of mold release (*case 2*), and (c) low thermal conductivity molds with high side rigidity and low stiction because of the presence of mold release (*case 3*). The specific mold release agent used is Huron Technologies, Inc. RC 6310 High Performance Silicone Mold Release and General Purpose Lubricant with 1 ml applied to the surface of the mold for case 1 and 3 ml applied for case 3. For all experiments, a thermoplastic polymer commonly used for molding processes, Low Density Polyethylene (LDPE) 722 from Dow Plastics, was employed. Three specimens were tested for each case.

To characterize the effects of a mold with low side rigidity in case 1, a 2.5 mm thick LDPE disc specimen with a 30.6 mm diameter was placed on a 3.2 mm thick piece of aluminum sheet since unconsolidated polymer granules [Fig. 4(a)]. It was necessary to hot-press the polymer granules into a disc specimen for the experiment, since it is

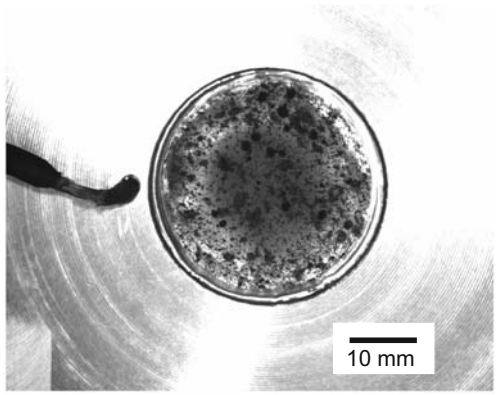

(a)

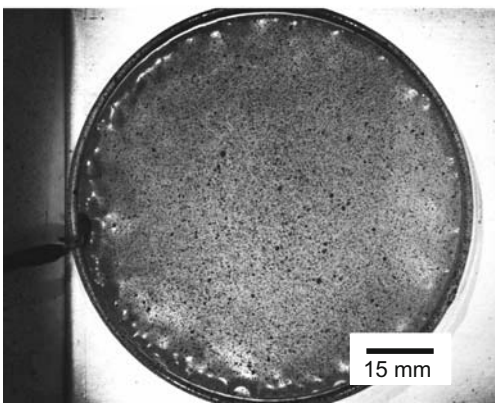

(b)

Fig. 4 Image of LDPE fully melted in (**a**) an aluminum mold and (**b**) a Pyrex Petri dish. Black spray paint has been applied to create the speckle pattern

very difficult for polymer granules to consolidate as they melt without enough side rigidity to hold them together during the melting process. To simulate variations in the cooling rate in the molding process for case 1, the sample was allowed to either air cool, or to cool quasi-steady state by reducing the temperature of the specimen in increments of 10°C and holding until the temperature of the specimen surface is uniform, as verified by infrared thermal measurements. To characterize the evolution of shrinkage during cooling, images were taken at intervals determined by the cooling rate. For cases 2 and 3, 20 g of 4 mm LDPE polymer granules were heated up inside of a 100 mm diameter Pyrex Petri dish, which had a flatness of better than 3 μm across the diameter, using a hot plate until fully melted into a 2.5 mm thick layer, and then allowed to cool by natural convection. Pyrex represents a molding material with a low coefficient of thermal expansion, thermal conductivity, and high rigidity. A sample image of fully melted LDPE just before the cooling process can be seen in Fig. 4(b).

Experimental Results

Results were obtained from three experimental conditions: (a) high thermal conductivity molds with low stiction and reduced side rigidity, (b) low thermal conductivity molds with low stiction and high side rigidity, and (c) low thermal conductivity molds with high stiction and high side rigidity. The results of each of the cases are discussed in detail in the following sections, and will be explained using a simple 1D model in the next section.

Case 1: Mold with High Thermal Conductivity and Reduced Side Rigidity

Because of the interaction between the polymer melt and the mold, experiments were initially conducted to decouple these effects from the strain measurements. These experiments unconstrained the polymer melt by placing it on a 1/8 in. thick aluminum plate with mold release to simulate a condition of reduced side rigidity for a mold with a high thermal conductivity and reduced side rigidity. DIC results for the shrinkage strain, which were found to be fairly reproducible between the three specimens tested under these conditions, can be seen in Fig. 5(a). It can be seen that there is a rapid 100% increase in the magnitude of the shrinkage strain observed around 115°C and another rapid 50% increase in the magnitude of the shrinkage strain around 70°C. These temperatures are very close to the melting point of 105°C, and Vicat softening point of 90°C respectively for the LDPE polymer. However, there is still a large shear strain that may be due to thermal gradients or stiction resulting from the rapid cooling. Thus, it would appear that the rapid increases are due to crystallization of the polymer at the melting point.

The relaxation of strain that occurs near the Vicat softening point, which is the temperature at which the material can be penetrated to a depth of 1 mm by a 1 kg load acting on a pin with a 1 mm^2 circular or square cross-section, is more difficult to explain. It is possible that thermal gradients result in the outer edges of the specimen shrinking and hardening more rapidly relative to the central region where the strain measurements are being obtained.

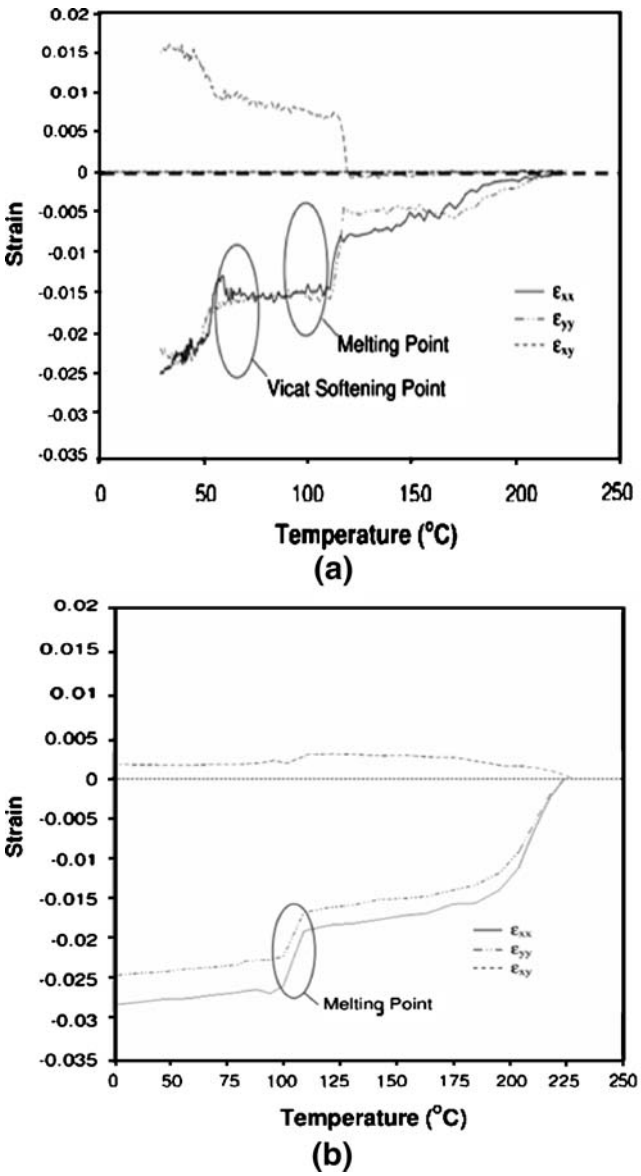

Fig. 5 Plot of the thermal evolution of shrinkage strain for (**a**) a hot-pressed disc of LDPE melted and then air cooled on an aluminum plate with mold release, and (**b**) a hot-pressed disc of LDPE melted and then cooling under quasi-steady state conditions by uniformly reducing the temperature of the specimen in 10°C increments on an aluminum plate with mold release (case 1)

Thus, the central region may be developing residual stresses due to differential shrinkage with the outer edges resulting from thermal gradients as the polymer rapidly cools below the Vicat softening point. Since the specimen should have very little constraint on any surface, the secant coefficient of thermal expansion (CTE), which is the total change in strain divided by the change in temperature, should be the close to the value reported by the manufacturer, which is 200 ppm/°C at room temperature. From Fig. 5(a), it can be seen that the secant CTE is approximately 125 ppm/°C at room temperature, which is 75 ppm/°C below the manufacturer reported value and is indicative of possible constraints due to thermal gradients. To directly confirm the presence of a thermal gradient, thermal measurements were taken at the center and edge of a specimen, and indicated the presence of a maximum 40°C temperature difference that rapidly occurs at the onset of cooling and then slowly diminishes as the temperature of the polymer approaches room temperature.

A second experiment was conducted using very controlled 10°C cooling steps that simulated a heated mold producing lower thermal gradients corresponding to a quasi-steady state cooling condition. The results for this experiment, seen in Fig. 5(b), indicate the presence of a small level of shear strain, about 0.25%, while the shrinkage strains rapidly develop to a magnitude of 1.5% after only 20°C of initial cooling as opposed to the more gradual increase observed in Fig. 5(a). Also, the sharp decrease at the Vicat softening point observed in Fig. 5(a) is not present in Fig. 5(b), indicating that there might be negligible residual stress accumulating that would otherwise result in a softening response. The secant CTE in the horizontal direction also increases to 150 ppm/°C, while in the vertical direction it is closer to the 125 ppm/°C observed from the experiments conducted using more rapid cooling. The difference in temperature between the edge and center of the specimen at the Vicat softening point is only 3°C in this case, which represents nearly a seven times decrease relative to the rapid cooling case. There is also an order of magnitude reduction in shear strain relative to the rapid cooling case. Thus, it appears that the constraint observed from the thermal gradient experienced during rapid cooling is alleviated during quasi-steady state cooling.

Case 2: Low Stiction with High Side Rigidity, Low Thermal Conductivity, and Low CTE

Case 2 involved melting pellets in a Pyrex Petri dish with high side rigidity, low thermal conductivity, and low CTE and air cooling to study how a homogeneous material shrinks in a mold due to air cooling during processing when mold release has been applied to the mold. Strain data was again obtained from the center of the image. The average value within the circular region for all of the deformed image strain contour plots was extracted and combined with the thermocouple data to indicate the thermal evolution of the shrinkage response in Fig. 6(a). Initially, the shrinkage strain develops very rapidly with cooling in both the horizontal and vertical directions to a magnitude of 1.5% to 2.0% after a temperature drop of only 25°C. The level of shear strain is much less than the normal strains, and is nearly constant for much of the cooling period. As the polymer melt continues to cool, the shrinkage strain increases almost linearly at a rate of 50 ppm/°C until a temperature of 110°C is reached. At this temperature there

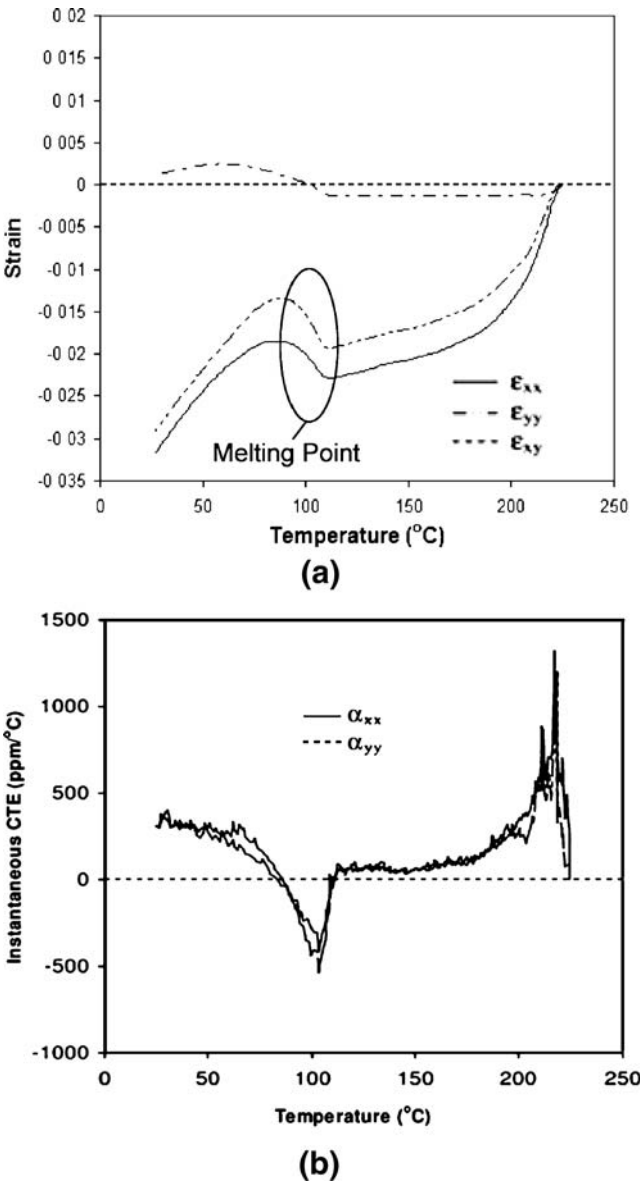

Fig. 6 Plot of the thermal evolution of (**a**) shrinkage strain in central region of the specimen formed by melting LDPE and then air cooling them in a Pyrex Petri dish with mold release, and (**b**) the instantaneous thermal expansion obtained from (**a**) (case 2)

is a sharp decrease, roughly 35%, in magnitude of the shrinkage strains. This is similar to the change in shrinkage strain seen in Fig. 5(a) at the temperature corresponding to the melting point of the polymer, except it appears the polymer chains may be relaxing in response to the side constraint from the mold as the polymer changes phase and solidifies, resulting in lower magnitude normal strains and shear deformation. As the specimen continues to cool, the polymer bonds quickly retract again, and continue to cause an overall shrinkage of the specimen. The final outcome of the data for the case of a homogeneous polymer with low stiction conditions shows an overall shrinkage on the order of 3% to 3.5%.

Changes in the thermomechanical response of a polymer can also be understood through the instantaneous CTE seen in Fig. 6(b), which is just the derivative of the strain in Fig. 6(a) obtained from a central finite-difference formula. The instantaneous CTE does vary substantially from approximately 1,200 to −500 ppm/°C, indicating that abrupt variations in thermal expansion that are four times the average need to be taken into account when molding polymer components. For a better understanding of the general thermomechanical response of the polymer, the secant CTE at room temperature was calculated and found to be approximately 165 ppm/°C in the horizontal direction and 150 ppm/°C in the vertical direction at room temperature. The secant CTE is consistent between the vertical and horizontal strain, indicating isotropic response, and compares favorably with the manufacturer reported CTE of 200 ppm/°C. However, the differences indicate that there is still substantial constraint of the polymer in the mold that is retarding the overall shrinkage of the polymer and producing a thermomechanical response that is generally the same as case 1, except that there is a rapid expansion rather than contraction at the melting point that is most likely due to a measured reversal in the thermal gradient between the center and edge of the specimen resulting from the presence of the sides of the mold.

Case 3: High Stiction with High Side Rigidity, Low Thermal Conductivity, and Low CTE

To study the effect of higher levels of stiction on the shrinkage response of a polymer melt, an experiment identical to the low stiction case was conducted without mold release. It is expected that the frictional and adhesive forces contributing to a high level of stiction that arises due to no mold release agent being present will constrain the deformation, resulting in less strain since the required forces developed in the polymer melt would have to overcome these frictional and adhesive forces. In a manner similar to case 2, a central circular region of the specimen was used to extract the average strain data to analyze with the corresponding temperature data, shown in Fig. 7(a). The data in this figure indicate a decrease in strain in both the horizontal and vertical directions as a result of the cooling, as was the case for lower levels of stiction. At first the decrease in normal strain occurs rapidly, and then slows down to a nearly constant level at 200°C, where the magnitude of the normal strains is on the order of 1.5%. The magnitudes of both curves agree very well up to this point, indicating that the normal strains are symmetric. The point at which there are jumps in both graphs corresponds to the point at which the central region of the polymer melt begins to change phase and solidify, approximately 110°C according to the thermocouple data. This temperature

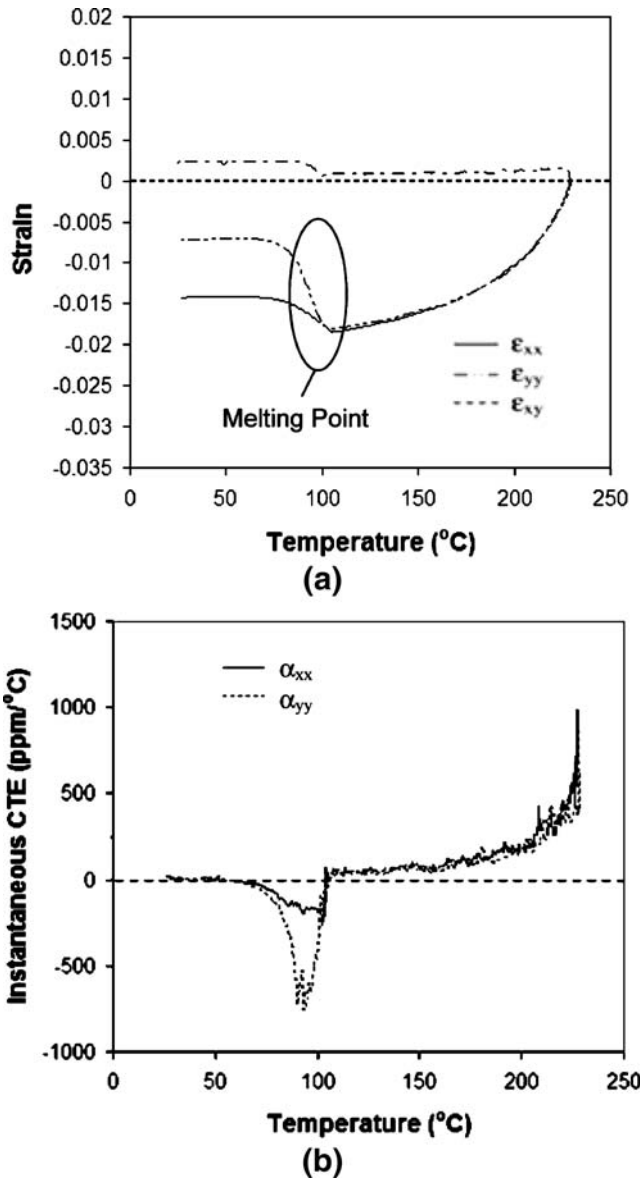

Fig. 7 Plot of the thermal evolution of (**a**) shrinkage strain in central region of the specimen for LDPE granules melted and then air cooled in a Pyrex Petri dish without mold release, and (**b**) the instantaneous coefficient of thermal expansion obtained from (**a**) (case 3)

agrees with the temperature where the phase change began in case 2. In the high stiction case, the change in strain due to the relaxation of the polymer chains is approximately 25% for the horizontal strain and near 40% for the vertical strains, but on the average the change in magnitude is close to what was seen in case 1.

The shear strain fluctuates up and down in a somewhat random pattern, but the overall trend is also a decrease as the temperature decreases after an initial jump, followed by a large jump that results in the shear strain doubling in magnitude and switching direction, from roughly −0.06% to 0.12%. This change is similar to that present in the low stiction case, and is consistent with the change from thermal contraction to expansion in the normal strains.

In a similar manner as was performed for the low stiction case, the instantaneous CTE was calculated [Fig. 7(b)]. It was found to vary between 1,000 and −700 ppm/°C, which is slightly less extreme levels of shrinkage than observed in the previous case. For this homogenous LDPE case with high stiction conditions, the secant CTE is calculated to be 75 ppm/°C in the horizontal direction and 38 ppm/°C in the vertical direction at room temperature. This is a remarkable difference in value from what was observed in the previous case; the stiction causes a drop in the apparent instantaneous CTE of approximately 50% to 75%. Furthermore, it would appear from Fig. 7(b) that the variation in CTE was very similar to case 2, except after solidification when the value does not change further. This has an important implication in the design of polymer components, where there may be a considerable amount of residual stress accumulating from the stiction between the polymer melt and the mold after solidification.

Modeling of Mold–Polymer Melt Interaction

In order to understand the experimental results of cases 1 though 3 in terms of the mold–polymer interaction, a simple 1D model was used based on the experimental observations. For case 1 where there is a steady-state cooling, it is assumed that the measured behavior is the actual thermal contraction behavior of the polymer. In order to model case 1 where there is a measured temperature difference (i.e., thermal gradient), it is assumed that the polymer can be divided into two regions: (a) one close to the mold which experiences rapid cooling due to the high thermal conductivity of the mold (region 1), and (b) a second being the majority of the polymer that is slowly air-cooled (region 2). The temperature difference between these two regions rapidly grows initially to the maximum measured temperature difference, and then slowly decreases as the temperature decreases. In this case, elastic stress equilibrium is assumed to exist between the two regions, with the modulus of each region increasing rapidly near the melting point and then more rapidly near the Vicat softening point. Thus, the measured strain in region 2, ε_2, that evolves in case 1 due to a time-dependent temperature difference is modeled as follows:

$$\varepsilon_2 = \frac{E(T_1(t)) \times \varepsilon(T_1(t)) \times (1-d) + E(T_2(t)) \times \varepsilon(T_2(t)) \times d}{(1-d) \times E(T_1(t)) + d \times E(T_2(t))} \tag{1}$$

where $E(T)$ is the modulus of the polymer at temperature T determined from thermomechanical analysis (TMA) as seen in Fig. 8(a), $\varepsilon(T)$ is the shrinkage strain at temperature T, T_1 and T_2 are the temperatures in each region at time t seen in Fig. 8(b), and d is the relative size of the air-cooled region taken to be 0.9.

For cases 2 (low stiction) and 3 (high stiction), equation 1 can also be used to model the shrinkage response. However, the polymer must be assumed to be of uniform temperature during cooling due to the low thermal conductivity of the mold. The interaction between the mold and polymer is assumed to be non-existent as the polymer initially cools. However, once the polymer solidifies (i.e., reaches the melting point) the interaction between the polymer and mold increases. For the case of no mold release, it is assumed that the mold constrains the shrinkage of the polymer. In the case of mold release, it is assumed that slippage gradually develops between the polymer and the mold, significantly reducing the constraint as the polymer hardens. This effect is modeled as an increase in effective temperature-dependent stiffness of the polymer region near the mold, $E_e(T)$, and a reduction in effective shrinkage, $\varepsilon_e(T)$, as follows:

$$E_e(T) = (1-\beta(T)) \times E(T) + \beta(T) \times E_m \tag{2a}$$

$$\varepsilon_e(T) = \varepsilon(T) \times (1-\beta(T)) + \varepsilon_m(T) \times \beta(T) \tag{2b}$$

where $\beta(T)$ is the interaction coefficient which varies with temperature as shown in Fig. 8(c), while E_m is the stiffness of the mold, which was taken to be 63 GPa, and $\varepsilon_m(T)$ is the thermal expansion of the mold, which is taken to be 3.3 ppm/°C times the change in temperature. The variation of $\beta(T)$ is chosen to reflect the expected variation of adhesion due to the mold release, and to provide reasonable correlation with the experimental data. Thus, the modeling of the constraint effect essentially treats the layer of polymer melt adjacent to the mold as a cohesive zone with rule of mixtures properties controlled by the interaction coefficient.

The predicted shrinkage of the polymer using the 1D model can be seen in Fig. 9. Comparing the predictions with the measured results in Figs. 5, 6(a), and 7(a), it can be seen that the model reasonably captures the observed trends of slow initial shrinkage with rapid increases near the

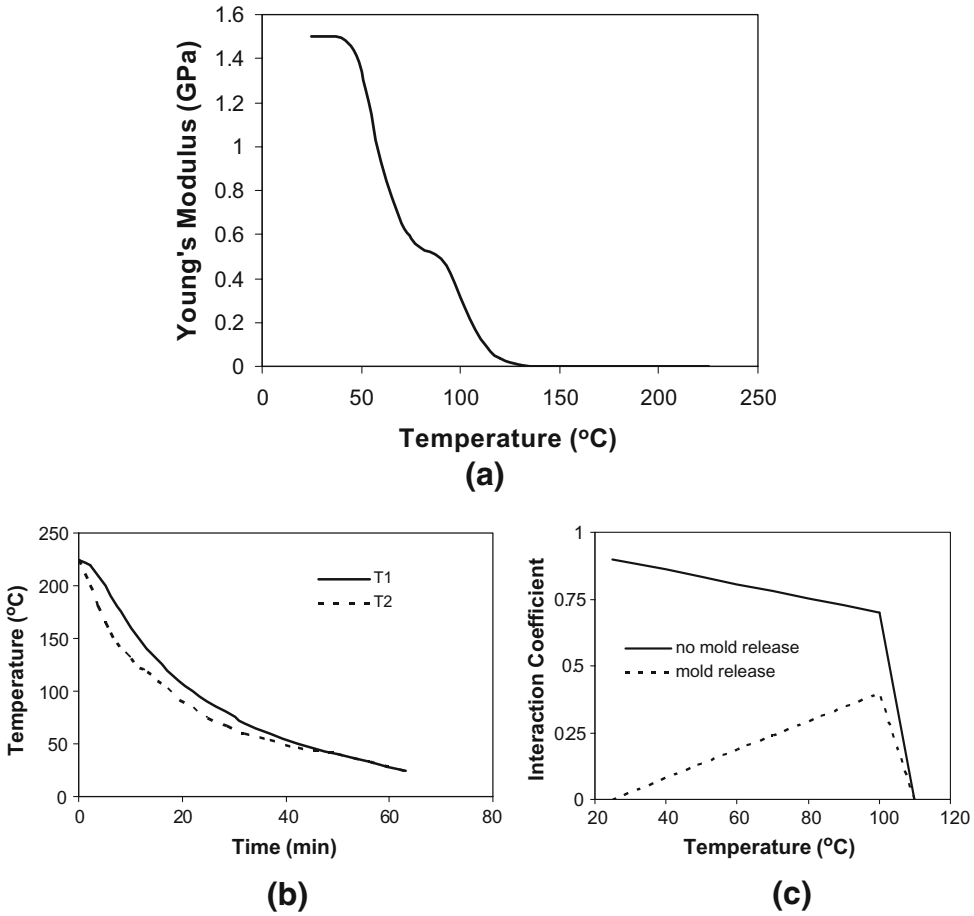

Fig. 8 Parameters used in the simple 1D model of shrinkage in equations 1 and 2: (**a**) temperature-dependent Young's modulus of polymer melt, (**b**) transient thermal profiles, $T_1(t)$ and $T_2(t)$, at the top and bottom of the polymer melt during rapid cooling, and (**c**) the stress transfer coefficient for the case of mold release and no mold release

melting point and Vicat softening point for case 1 where there is rapid cooling and therefore a substantial temperature difference. For case 2, the rapid decrease at the melting point and subsequent recovery due to slippage can also be captured, while the constraint in case 3 causes greater decrease and no recovery. In all cases, the levels at which these changes occur are also reasonably captured. Thus, it appears that the experimental results can be reasonably explained and predicted using the simple 1D model.

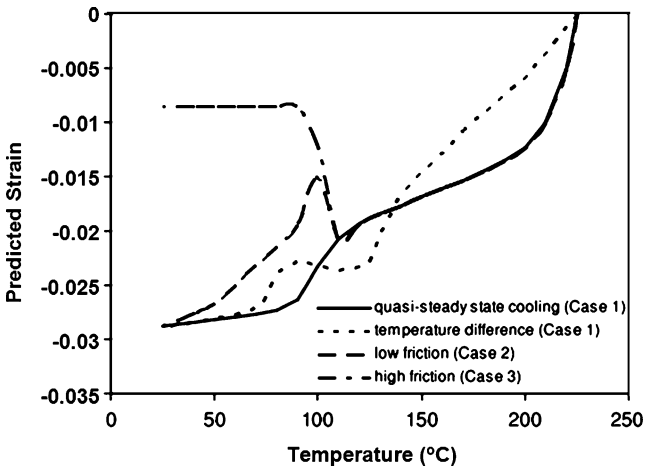

Fig. 9 Predicted shrinkage behavior using a 1D model for the interaction of the polymer and mold based on the steady-state cooling behavior of the polymer (case 1) that accounts for temperature difference in the polymer due to the high thermal conductivity of the mold (case 1), the elimination of stiction between the polymer and a low thermal conductivity mold using mold release (case 2), and the effect of the stiction between the polymer and low thermal conductivity mold (case 3)

Conclusions

New in situ open mold experiments have been designed for the first time to measure deformations associated with the shrinkage of thermoplastic polymers in traditional and emerging molding processes. The new experiments consist of the full-field deformation technique of Digital Image Correlation (DIC) to characterize the displacement and corresponding strain fields that evolve as the polymer shrinks from the molten to the solid state during molding processes, simulated open molds, a heating stage, and thermocouples for temperature measurements.

From these experiments, it has been shown that there are large variations in shrinkage strain associated with the transition of the polymer from the molten to the solid state resulting in instantaneous CTEs of 1,200 to −700 ppm/°C.

Rapidly cooling the polymer resulted in another substantial increase in instantaneous CTE corresponding to 1,000 ppm/°C near the Vicat softening point. A secant CTE is measured in the polymer of 150 to 165 ppm/°C, which is similar to that reported by the manufacturer. However, increasing the rigidity of the mold and stiction substantially reduced the shrinkage strain and corresponding secant CTE to the range of 38 to 75 ppm/°C. A simple 1D model of the mold–polymer melt interaction reasonably explained the observed trends in the shrinkage behavior by attributing them to temperature differences through the thickness of the polymer melt when using high conductivity molds as well as constraint in the polymer melt near the mold resulting from stiction.

Acknowledgements This work was supported by NSF grants EEC0315425 and DMI0457058, and by ONR award number N000140710391. Opinions expressed in this paper are those of the authors and do not necessarily reflect opinions of the sponsors.

References

1. Ananthanarayanan A, Gupta SK, Bruck HA, Yu Z, Rajurkar KP (2007) Development of in-mold assembly process for realizing mesoscale revolute joints. North American Manufacturing Research Conference, Ann Arbor MI, USA, pp 1–8.
2. Banerjee A, Li X, Fowler G, Gupta SK (2007) Incorporating manufacturability considerations during design of injection molded multi-material objects. Res Eng Des 17:207–231.
3. Gouker RM, Gupta SK, Bruck HA, Holzschuh T (2006) Manufacturing of multi-material compliant mechanisms using multi-material molding. Int J Adv Manuf Technol 28:1–27.
4. Priyadarshi AK, Gupta SK, Gouker R, Krebs F, Shroeder M, Warth S (2007) Manufacturing multi-material articulated plastic products using in-mold assembly. Int J Adv Manuf Technol 32:350–365.
5. Ananthanarayanan A., Thamire C, Gupta SK (2007) Investigation of revolute joint clearances created by in-mold assembly process. IEEE International Symposium on Assembly and Manufacturing, Ann Arbor, Michigan, pp 26–134.
6. Bushko WC, Vijay K (1996) Stokes solidification of thermoviscoelastic melts. Part 4: Effects of boundary conditions on shrinkage and residual stresses. Polym Eng Sci 36:658–675.
7. Titomanlio G, Jansen KMB (1996) In-mold shrinkage and stress prediction in injection molding. Polym Eng Sci 38:2041–2049.
8. Jansen KMB, Titomanlio G (1996) Effect of pressure history on shrinkage and residual stresses-injection molding with constrained shrinkage. Polym Eng Sci 36:1537–1550.
9. Jansen KMB, Van Dijk DJ, Husselman MH (1998) Effect of processing conditions on shrinkage in injection molding. Polym Eng Sci 38:838–846.
10. Kramschuster A, Cavitt R, Ermer D, Chen Z, Turng L-S (2005) Quantitative study of shrinkage and warpage behavior for microcellular and conventional injection molding. Polym Eng Sci 45:1408–1418.
11. Liao SJ, Chang DY, Chen HJ, Tsou LS, Ho JR, Yau HT, Hsieh WH (2004) Optimal process conditions of shrinkage and warpage of thin-wall parts. Polym Eng Sci 44:917–928.
12. Pontes AJ, Pouzada AS (2004) Ejection force in tubular injection moldings. Part I: Effect of processing conditions. Polym Eng Sci 44:891–898.
13. Han S, Wang KK (1997) Shrinkage prediction for slowly crystallizing thermoplastic polymers in injection molding. Int Polym Process, XII, 12:228–237.
14. Delaunay D, Le Bot P (2000) Nature of contact between polymer and mold in injection molding. Part II: Influence of mold deflection on pressure history and shrinkage. Polym Eng Sci 40:1682–1691.
15. Kwon K, Isayev AI, Kim KH (2005) Toward a viscoelastic modeling of anisotropic shrinkage in injection molding of amorphous polymers. J App Polym Sci 98:2300–2313.
16. Bruck HA, Fowler G, Gupta SK, Valentine T (2004) Using geometric complexity to enhance the interfacial strength of heterogeneous structures fabricated in a multi-stage, multi-piece molding process. Exp Mech 44:261–271.
17. Egan E, Amon CH (2000) Thermal management strategies for embedded electronic components of wearable computers. J Electron Packag 122:98–106.
18. Goodship V, Love JC (2002) Multi-material injection molding. ChemTec Publishing, Toronto.
19. The NJ, Conway PP, Palmer PJ, Prosser S, Kioul A (2000) Statistical optimisation of thermoplastic injection moulding process for the encapsulation of electronic subassembly. J Electron Manuf 10:171–179.
20. Sarvar F, Teh NJ, Whalley DC, Hunt DC, Palmer DA, Wolfson PJ (2004) Thermo-mechanical modelling of polymer encapsulated electronics. IEEE Intersociety Conference on Thermal Phenomena. Las Vegas, NV 2:465–472.
21. Bruck HA, Schreier HW, Sutton MA, Chao YJ (1997) Development of a Measurement System for Combined Temperature and Strain Measurements During Welding," Technology Advancements and New Industrial Applications in Welding, pp. 523–526.
22. Bruck HA, McNeill SR, Sutton MA, Peters WH III (1989) Digital image correlation using Newton-Raphson method of partial differential correction. Exp Mech 29:261–267.
23. Sutton MA, Turner JL, Bruck HA, Chae TL (1991) Full-field representation of discretely sampled surface deformation for displacement and strain analysis. Exp Mech 31:168–177.
24. Helm JD, McNeill SR, Sutton MA (1996) Improved three-dimensional image correlation for surface displacement measurement and strain analysis. Opt Eng 35:1911–1920.
25. Luo PF, Chao YJ, Sutton MA, Peters WH III (1993) Accurate measurement of three-dimensional deformations in deformable and rigid bodies using computer vision. Exp Mech 33:123–132.
26. Schreier HW, Braasch JR, Sutton MA (2000) Systematic errors in digital image correlation caused by intensity interpolation. Opt Eng 39:2915–2921.